Journal of Technomaterial Physics
Journal homepage: https://talenta.usu.ac.id/JoTP

Influence of Mode of Hydrothermal Treatment and Precursor State on Phase Formation and Crystallinity of Sodium Titanate

Ervina Putri Wulandari[1], Zikri Noer[2,3,4,5*], Martha Rianna[1,6], Syahrul Humaidi[1,6], Muhammad Abduh Akram Agus[1,5], Alya Nazwariva[3] and Jihan Murtadha Rambe[2,5]

[1] *Master's Program in Physics, Department of Physics, Faculty of Mathematics and Natural Sciences, Universitas Sumatera Utara, Jl. Bioteknologi No. 1, Medan 20155, North Sumatra, Indonesia*
[2] *Study Program of Instrumentation Engineering Technology, Faculty of Vocational, Universitas Sumatera Utara, Jl. Bioteknologi No. 2, Medan, 20155, North Sumatra, Indonesia*
[3] *Diploma Program in Physics, Faculty of Vocational, Universitas Sumatera Utara, Jl. Bioteknologi No. 2, Medan 20155, North Sumatra, Indonesia*
[4] *Center of Excellence for Functional Materials and Instrumentation, Universitas Sumatera Utara, Medan, 20155, North Sumatra, Indonesia*
[5] *Sustainable Energy and Advanced Functional Materials (SEAM), Faculty of Vocational, Universitas Sumatera Utara, Jl. Bioteknologi No. 2, Medan, 20155, North Sumatra, Indonesia*
[6] *Department of Physics, Faculty of Mathematics and Natural Sciences, Universitas Sumatera Utara, Jl. Bioteknologi No. 1, Medan, 20155, North Sumatra, Indonesia*

[*]Corresponding Author: zikrinoer@usu.ac.id

ARTICLE INFO

Article history:
Received 09 February 2026
Revised 03 April 2026
Accepted 20 April 2026
Available online 02 May 2026

E-ISSN: 2656-0755
P-ISSN: 2656-0747

How to cite:
E. P. Wulandari, Z. Noer, M. Rianna, S. Humaidi, M. A. A. Agus, A. Nazwariva, and J. M. Rambe, "Influence of Mode of Hydrothermal Treatment and Precursor State on Phase Formation and Crystallinity of Sodium Titanate," Journal of Technomaterial Physics, vol. 08, no. 01, pp. 50–58, Feb. 2026, doi: 10.32734/jotp.v8i1.24729.

ABSTRACT

Sodium titanate was synthesized via a sol–gel-assisted hydrothermal method to study phase evolution and crystallinity under different hydrothermal treatment conditions and precursor compositions. Four processing routes were designed: continuous hydrothermal treatment (24 h), interrupted hydrothermal cycles (3 × 8 h), dried-gel hydrothermal treatment, and fresh-gel hydrothermal treatment. X-Ray Diffraction (XRD) was used to analyze the resulting crystal phases and crystallite sizes. Continuous treatment of fresh gel produced monoclinic $Na_2Ti_6O_{13}$ with small crystallites (12.4 nm), while interrupted processing increased crystallite size to 15.5 nm. Pre-drying of the sol–gel precursor prior to continuous hydrothermal treatment yielded well-defined $Na_2Ti_6O_{13}$ with enhanced crystallinity and larger crystallites (27.6 nm). In contrast, insufficient precursor stabilization redirected phase evolution toward monoclinic Na_2TiO_3 despite comparable crystallite size. The results demonstrate that the hydrothermal treatment mode primarily governs crystallite growth, whereas the precursor state controls phase selectivity. These findings provide a clear synthesis–structure relationship for tailoring sodium titanate materials.

Keywords: Sodium Titanate, Sol-Gel, Hydrothermal, Crystal Structure Characterization, X-Ray Diffraction (XRD).

ABSTRAK

Sodium titanat disintesis menggunakan metode hidrotermal berbantuan sol–gel untuk mengkaji evolusi fasa dan kristalinitas pada berbagai kondisi perlakuan hidrotermal dan keadaan prekursor. Empat variasi proses diterapkan, yaitu: hidrotermal kontinu selama 24 jam, hidrotermal terputus dalam tiga siklus masing-masing 8 jam, hidrotermal menggunakan prekursor gel yang telah dikeringkan, dan hidrotermal menggunakan gel segar. Analisis difraksi sinar-X (XRD) menunjukkan bahwa kontinuitas hidrotermal dan kondisi prekursor secara signifikan memengaruhi pertumbuhan kristalit dan selektivitas fasa. Perlakuan kontinu terhadap gel segar menghasilkan $Na_2Ti_6O_{13}$ monoklinik dengan ukuran kristalit relatif kecil (12,4 nm), sedangkan perlakuan terputus meningkatkan ukuran kristalit menjadi 15,5 nm. Pengeringan prekursor sol–gel sebelum proses

hidrotermal menghasilkan $Na_2Ti_6O_{13}$ yang terdefinisi dengan baik, dengan kristalinitas lebih tinggi dan ukuran kristalit lebih besar (27,6 nm). Sebaliknya, stabilisasi prekursor yang tidak memadai mengarahkan evolusi fasa menuju Na_2TiO_3 monoklinik meskipun ukuran kristalitnya sebanding. Hasil ini menunjukkan bahwa kontinuitas hidrotermal terutama mengontrol pertumbuhan kristalit, sedangkan kondisi prekursor menentukan selektivitas fasa. Temuan ini memberikan pemahaman yang jelas mengenai hubungan antara parameter sintesis dan struktur kristal dalam rekayasa material sodium titanat.

Kata kunci: Sodium Titanat, Sol-Gel, Hidrotermal, Karakterisasi Struktur Kristal, Difraksi Sinar-X (XRD).

1. Introduction

Fossil fuels remain the dominant global energy source. However, their continued consumption has resulted in severe environmental challenges, including greenhouse gas emissions, air pollution, and climate change [1–3]. The increasing penetration of renewable energy sources such as solar and wind power introduces intermittency and grid instability, thereby necessitating reliable energy storage systems (ESS) to balance supply and demand [4-5]. Among various ESS technologies, rechargeable electrochemical batteries are particularly attractive due to their high energy efficiency, flexibility, and scalability [6].

Although lithium-ion batteries (LIBs) dominate the current market, concerns about lithium resource availability, uneven geographic distribution, and rising costs have spurred interest in alternative systems for large-scale applications [7–8]. Sodium-ion batteries (SIBs) have emerged as promising candidates because sodium is abundant, widely distributed, and economically favorable [9–11]. However, the larger ionic radius of Na^+ compared to Li^+ presents challenges in identifying suitable host structures that enable stable and reversible intercalation.

Sodium titanate compounds, particularly $Na_2Ti_6O_{13}$ and $Na_2Ti_3O_7$, have attracted significant attention as potential anode materials for sodium-ion batteries owing to their open-tunnel or layered crystal structures, structural stability, and relatively low operating voltage [11–12]. $Na_2Ti_6O_{13}$ possesses a monoclinic tunnel-type framework that facilitates Na^+ diffusion while maintaining mechanical integrity during repeated charge–discharge cycles [12–14]. Various synthesis routes for sodium titanate have been reported, including solid-state reactions, conventional hydrothermal methods, microwave-assisted hydrothermal synthesis, sol-gel methods, and other solution-based processes [15]. These studies demonstrate that synthesis parameters such as temperature, alkaline concentration, and calcination conditions strongly influence phase formation and crystallinity.

Among these approaches, sol–gel-assisted hydrothermal synthesis offers advantages, including improved precursor homogeneity, enhanced molecular-level chemical mixing, and better control over nucleation and crystal growth compared to conventional solid-state reactions. While several studies have explored hydrothermal temperature, reaction time, and NaOH concentration in sodium titanate synthesis, comparative investigations of precursor condensation state (fresh gel versus dried gel) and hydrothermal treatment mode (continuous versus interrupted) remain limited, particularly for the formation of $Na_2Ti_6O_{13}$. The influence of these two parameters on crystallite growth behavior and structural ordering has not been systematically clarified [15].

The physical state of the precursor can significantly affect nucleation kinetics and cation distribution during hydrothermal processing. Drying the gel prior to hydrothermal treatment may enhance polymer network condensation and chemical homogeneity, potentially promoting synchronized crystal growth. Conversely, interruption of hydrothermal treatment may induce repeated nucleation events and defect formation, thereby affecting crystallite size and structural ordering [16,19,24]. Understanding the roles of these synthesis variables is therefore essential for tailoring the crystal structure of sodium titanate.

In this study, sodium titanate was synthesized via a sol–gel assisted hydrothermal method using four processing routes designed to isolate the effects of (i) hydrothermal continuity and (ii) precursor state. The resulting materials were calcined and structurally characterized using X-ray diffraction (XRD) to evaluate phase formation and crystallinity. By systematically comparing these two synthesis variables, this work aims to clarify their influence on the development of $Na_2Ti_6O_{13}$ crystals and to provide fundamental insight into synthesis–structure relationships relevant to sodium-ion battery materials.

2. Method

2.1. Materials

Titanium(IV) isopropoxide (TTIP, 97%, Sigma-Aldrich), sodium hydroxide (NaOH pellets, 98%, Merck), citric acid ($C_6H_8O_7$, 99.5%, Merck), and ethylene glycol ($C_2H_6O_2$, 99%, Merck) were used as received without further purification. Deionized water was used in all solution preparations.

2.2. Sol-Gel Preparation

The precursor was synthesized via a citrate-assisted sol–gel route. NaOH was first dissolved in deionized water to prepare the sodium solution. Citric acid was then added at a Na^+: citric acid molar ratio of 1:2 under magnetic stirring for 30 min at room temperature to form a sodium–citrate complex. Separately, TTIP was dissolved in ethylene glycol at a Ti^{4+}: ethylene glycol molar ratio of 1:5 under continuous stirring to improve stability and minimize premature hydrolysis. The TTIP solution was added dropwise into the sodium–citrate solution under stirring at 70 °C. The mixture was maintained at 70 °C for 2 h to promote chelation and polymer network formation. The temperature was subsequently increased to 80–90 °C until a homogeneous gel was obtained.

2.3. Mode of Hydrothermal Treatment Variation

To evaluate the influence of hydrothermal treatment mode on sodium titanate formation, freshly prepared gel precursors were dispersed in 2 M NaOH solution and transferred into a Teflon-lined stainless-steel autoclave. Two hydrothermal conditions were applied at 180 °C:

a. Continuous hydrothermal treatment for 24 h.
b. Interrupted hydrothermal treatment consisting of three cycles of 8 h each with natural cooling between cycles.

After hydrothermal processing, the products were washed with deionized water until the pH was neutral and dried at 100 °C for 12 h.

2.4. Precursor State Variation

To investigate the influence of the precursor state, two precursor conditions were prepared: dried gel and fresh gel. Both precursors were subjected to continuous hydrothermal treatment at 180 °C for 24 h under identical conditions to ensure a fair comparison.

2.5. Calcination Process

The dried hydrothermal products were calcined at 800 °C for 3 h in air using a furnace, with a heating rate of 5 °C min^{-1}. The furnace was allowed to cool naturally to room temperature.

2.6. Structural characterization

The crystal structure of the synthesized powders was analyzed using X-ray diffraction (XRD) on an X'Pert PRO MPD diffractometer (PANalytical) equipped with Cu Kα radiation (λ = 1.5406 Å). The instrument was operated at 40 kV and 30 mA. Diffraction patterns were recorded over a 2θ range of 10°–80° with a step size of 0.02°.

Phase identification was performed by comparison with standard reference patterns from the ICDD PDF database. Peak indexing and data analysis were conducted using HighScore Plus software.

The crystallite size (D) was estimated using the Scherrer equation (Eq. 1):

$$D = \frac{K\lambda}{\beta \cos \theta} \quad (1)$$

where K is the shape factor (0.9), λ is the X-ray wavelength (1.5406 Å), β is the full width at half maximum (FWHM) in radians, and θ is the Bragg angle.

3. Results and Discussion

3.1. Effect of Mode of Hydrothermal Treatment

To elucidate the role of hydrothermal continuity in structural development, the crystalline phases from continuous and interrupted hydrothermal treatments were compared using X-ray diffraction. The obtained patterns reveal that both synthesis routes successfully yield sodium titanate corresponding to monoclinic $Na_2Ti_6O_{13}$, indicating that hydrothermal processing, continuous or interrupted hydrothermal treatment, is sufficient to induce phase transformation of the sol–gel precursor into the titanate framework [16-17].

The X-ray diffraction patterns were recorded in the 2θ range of 10°–80°. For the sample obtained by continuous hydrothermal treatment (Figure 1), the diffraction peaks are indexed to monoclinic $Na_2Ti_6O_{13}$ in agreement with PDF No. 00-014-0277. The characteristic reflections at 2θ = 11.8° (200), 24.5° (110), 29.8° (310), 30.1° (20–3), 30.5° (31–1), 33.4° (402), 43.3° (40–4), 44.2° (602), and 48.6° (020) confirm the formation of the layered/tunnel titanate structure. However, the peaks appear noticeably broadened and are superimposed on a relatively elevated low-angle background. Such features typically indicate incomplete structural condensation and the presence of partially disordered or amorphous domains originating from the direct use of fresh sol–gel precursor without prior stabilization. The absence of a drying stage may lead to compositional heterogeneity and asynchronous nucleation during hydrothermal processing, thereby limiting coherent crystallite growth [18-19].

In addition to the main diffraction peaks, a minor reflection observed around 2θ = 15° may be associated with layered sodium titanate phases such as $Na_2Ti_3O_7$, which are commonly formed as intermediate structures during hydrothermal synthesis. This suggests that the phase transformation toward the tunnel-type $Na_2Ti_6O_{13}$ is not fully completed under certain processing conditions. Meanwhile, the feature near 2θ = 35° is likely attributed to overlapping reflections or lattice distortions resulting from limited crystallinity and structural disorder. Such behavior is typical in nanocrystalline titanate systems synthesized under kinetically constrained conditions. Furthermore, weak reflections observed in the 50–65° range correspond to high-index crystallographic planes with low intensity and do not indicate the presence of significant impurity phases. These observations confirm that the additional reflections are related to structural features rather than to impurity phases [18-20].

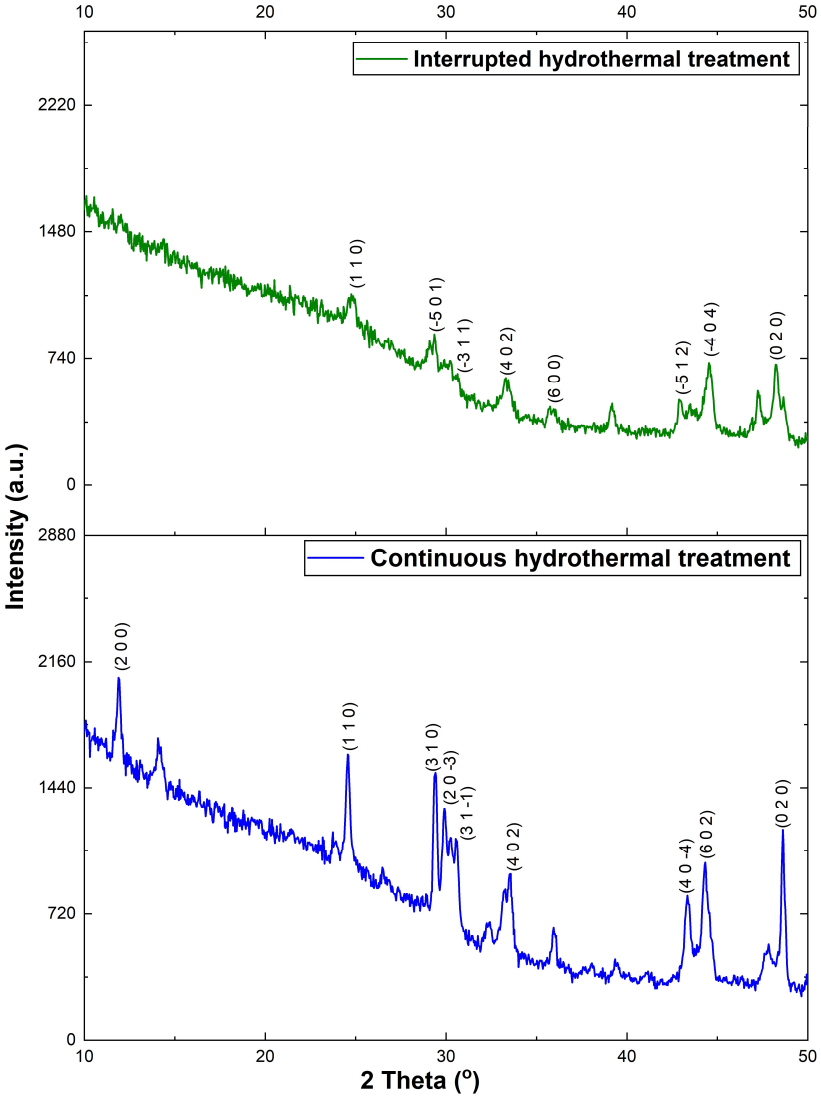

Figure 1. XRD patterns of samples obtained by continuous hydrothermal treatment and interrupted hydrothermal treatment

Quantitative peak profile analysis of the most intense reflection at 2θ = 33.6° yields a full width at half maximum (FWHM) of 0.669° (2θ). Based on the Scherrer equation (Eq. 1), the calculated average crystallite size is approximately 12.4 nm, confirming that the sample obtained by continuous hydrothermal treatment consists of nanocrystalline domains with restricted long-range ordering. The relatively large FWHM supports the notion that crystal growth is kinetically constrained under this processing condition.

In contrast, the sample obtained by interrupted hydrothermal treatment also crystallizes as monoclinic $Na_2Ti_6O_{13}$, consistent with PDF No. 00-037-0951. The diffraction positions closely match the standard reflections at 2θ = 11.8°, 24.5°, 30.0°, 30.5°, 33.5°, 35.2°, 41.3°, 43.4°, 44.3°, 47.9°, and 48.7°, corresponding to the characteristic planes of the tunnel-type titanate framework. The crystallographic parameters (a = 15.120 Å, b = 3.738 Å, c = 9.160 Å, β = 99.3°) are consistent with the reported monoclinic structure of $Na_2Ti_6O_{13}$.

Although the interrupted hydrothermal treatment sample (Figure 1) exhibits sharper reflections than the continuous hydrothermal treatment sample, slight peak broadening is still observed at the reflection around 2θ ≈ 33° relative to fully continuous processing. The segmented hydrothermal schedule likely induces repeated nucleation upon reheating, partially interrupting sustained crystal growth. Nevertheless, the measured FWHM at 2θ = 33.3° decreases to 0.535° (2θ), corresponding to an average crystallite size of approximately 15.5 nm. This increase in crystallite dimension relative to the continuous hydrothermal treatment sample indicates that partial structural reorganization occurs during each cycle, allowing moderate grain growth despite the interruption [20].

From a mechanistic standpoint, the mode of hydrothermal treatment strongly influences nucleation–growth balance. In the sample obtained by continuous hydrothermal treatment, direct treatment of the unstabilized precursor promotes rapid nucleation but limited growth, resulting in smaller crystallites and higher structural disorder. Conversely, the interrupted hydrothermal strategy in the sample obtained via interrupted hydrothermal treatment permits intermittent structural relaxation and ionic species redistribution during cooling–reheating cycles, facilitating incremental crystallite coarsening. However, because the process is not fully continuous, complete long-range ordering is not achieved [21].

Comparatively, the crystallite size trend (12.4 nm for continuous hydrothermal treatment < 15.5 nm for interrupted hydrothermal treatment) demonstrates that sustained hydrothermal exposure promotes more effective atomic diffusion and octahedral reorganization within the TiO_6 framework. Continuous thermal energy input enhances crystal ripening and reduces microstrain, leading to narrower diffraction peaks and improved structural coherence.

Overall, these findings clearly demonstrate that hydrothermal continuity plays a critical role in controlling crystallographic ordering, crystallite growth, and nanostructural evolution in $Na_2Ti_6O_{13}$. While both interrupted and non-dried routes successfully produce the monoclinic titanate phase, continuous processing provides a more favorable environment for long-range structural development and enhanced crystallinity.

3.2. Effect of Precursor State

The X-ray diffraction (XRD) pattern of the dried gel sample, synthesized from a dried sol–gel precursor followed by continuous hydrothermal treatment at 180 °C for 24 h and subsequent calcination at 800 °C, confirms the formation of monoclinic $Na_2Ti_6O_{13}$ as the dominant crystalline phase. The major diffraction peaks exhibit excellent agreement with the standard reference card (PDF No. 00-037-0951), particularly the reflections at 2θ = 24.6°, 29.9°, 33.1°, 35.2°, and 48.7°, which are characteristic of the tunnel-type $Na_2Ti_6O_{13}$ framework. In addition, a pronounced reflection observed around 2θ ≈ 43° corresponds to the (404) plane of monoclinic $Na_2Ti_6O_{13}$, while several reflections appearing within the 45–65° range are associated with higher-index planes of the tunnel-type $Na_2Ti_6O_{13}$ structure. The relatively high peak intensity and sharp diffraction profiles indicate well-developed long-range crystallographic ordering [22].

Compared with samples derived from fresh gel or subjected to interrupted hydrothermal cycles, the dried gel sample exhibits noticeably narrower diffraction peaks and a reduced background signal. This behavior reflects enhanced crystallographic coherence and minimal amorphous contribution. The pre-drying step at 120 °C likely promotes partial condensation of the citrate–ethylene glycol polymeric network, thereby improving precursor homogeneity and more uniform Na^+/Ti distribution prior to hydrothermal crystallization. Such stabilization enables synchronous nucleation and sustained crystal growth during hydrothermal processing, which is further consolidated during high-temperature calcination [23].

Quantitative peak profile analysis of the dominant reflection at 2θ = 33.1° yields a full width at half maximum (FWHM) of approximately 0.301° (2θ). Based on Equation (1), the calculated average crystallite size is about 27.6 nm. The relatively narrow peak width and increased crystallite dimension compared to continuous hydrothermal treatment and interrupted hydrothermal treatment demonstrate that precursor pre-

drying significantly enhances crystal growth kinetics and reduces structural disorder. These findings confirm that precursor conditioning plays a crucial role in promoting the formation of well-defined $Na_2Ti_6O_{13}$ tunnel structures [24-25].

In contrast, the XRD pattern of the fresh gel sample (Figure 2) reveals a distinct phase evolution pathway. Search–match analysis indicates that the diffraction peaks are best indexed to monoclinic Na_2TiO_3 (PDF No. 00-037-0346), rather than $Na_2Ti_6O_{13}$. The experimental peak positions closely coincide with the strongest reflections of Na_2TiO_3, while the characteristic reflections associated with the tunnel-type $Na_2Ti_6O_{13}$ phase are absent or significantly suppressed. In particular, a noticeable reflection around $2\theta = 42°$ is likely associated with intermediate titanate-related phases, indicating that the phase transformation is not fully completed in the fresh gel sample. Furthermore, additional weak reflections observed in the 50–70° region are associated with high-index crystallographic planes with inherently low intensity and do not indicate the presence of impurity phases [26-27].

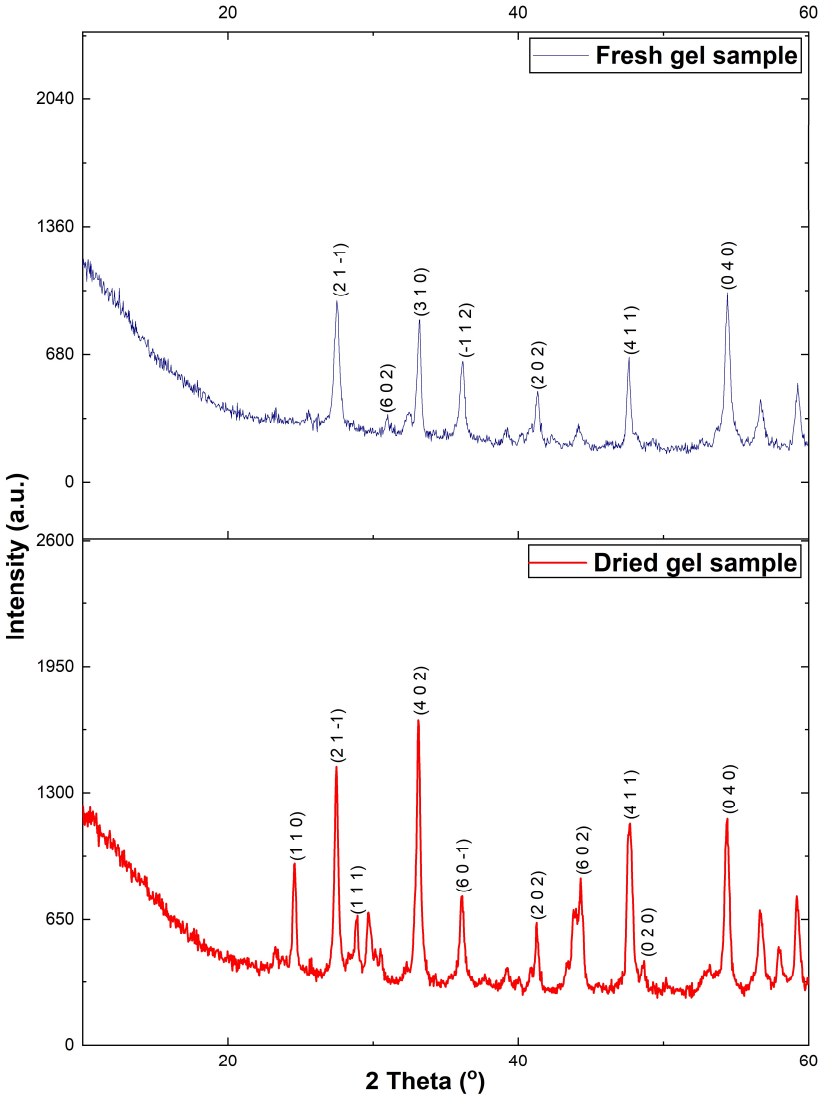

Figure 2. XRD patterns of the dried gel and fresh gel sample

Despite being subjected to similar hydrothermal and calcination temperatures, the precursor state fundamentally alters phase selectivity. In sodium titanate systems, the transformation toward $Na_2Ti_6O_{13}$ requires extensive reorganization of TiO_6 octahedra into a tunnel-type architecture. If precursor condensation and ionic redistribution are insufficiently controlled, the system may instead stabilize Na_2TiO_3, which possesses a comparatively simpler layered framework and may be kinetically favored under certain Na activity and alkalinity conditions [28-29].

Peak fitting of the dominant reflection at $2\theta = 33.2°$ in the fresh gel sample yields a FWHM of 0.301° (2θ), corresponding to a crystallite size of approximately 27.6 nm. Although the crystallite dimension is comparable

to that of the dried gel sample, the crystal phase differs fundamentally, with the fresh gel sample forming monoclinic Na_2TiO_3 rather than the tunnel-type $Na_2Ti_6O_{13}$ structure observed in dried gel sample. This observation indicates that crystallite size alone does not determine phase identity; instead, phase evolution is governed by precursor chemistry, sodium activity, and the structural rearrangement pathway during hydrothermal treatment [26,29]

Overall, the comparative analysis demonstrates that precursor drying combined with continuous hydrothermal processing promotes the formation of the tunnel-type $Na_2Ti_6O_{13}$ phase with enhanced structural ordering. Conversely, insufficient precursor stabilization may redirect crystallization toward monoclinic Na_2TiO_3, even when crystallinity remains relatively high. These findings emphasize the strong sensitivity of sodium titanate phase evolution to precursor state and hydrothermal kinetics, underscoring the necessity of controlled processing conditions to selectively obtain the desired $Na_2Ti_6O_{13}$ structure.

From a mechanistic perspective, the formation of $Na_2Ti_6O_{13}$ from sodium titanate precursors can be interpreted as a kinetically controlled structural rearrangement process. Under hydrothermal conditions, Na–Ti–O species initially nucleate into relatively simple titanate frameworks, such as Na_2TiO_3, which possess layered or less complex octahedral connectivity. The transformation toward $Na_2Ti_6O_{13}$ requires extensive reorganization of TiO_6 octahedra into a tunnel-type architecture through condensation and edge-sharing rearrangements. This process involves atomic diffusion, redistribution of Na^+ ions within interstitial channels, and partial dissolution–recrystallization under alkaline conditions [30-31].

Thermodynamically, $Na_2Ti_6O_{13}$ is stable at elevated temperatures; however, kinetically, its formation demands sufficient structural mobility and sustained energy input to enable octahedral reconfiguration. If hydrothermal treatment is continuous and the precursor network is adequately stabilized (as in dried gel), synchronized nucleation and prolonged crystal growth allow progressive ordering and eventual stabilization of the tunnel framework. Conversely, when precursor condensation is incomplete or sodium activity is locally high (as in fresh gel), the system may become kinetically trapped in the simpler Na_2TiO_3 structure. In such cases, insufficient octahedral rearrangement prevents the structural transition toward $Na_2Ti_6O_{13}$ despite comparable crystallite sizes.

Therefore, the evolution from Na_2TiO_3 to $Na_2Ti_6O_{13}$ can be regarded as a diffusion-controlled, structurally reconstructive transformation governed by precursor homogeneity, sodium availability, and hydrothermal continuity. The ability to direct phase selectivity thus depends not only on temperature and duration but also on the kinetic pathway dictated by precursor chemistry and processing sequence. These observations confirm that the additional reflections are intrinsic to sodium titanate structures rather than impurity phases.

4. Conclusion

This study demonstrates that the hydrothermal treatment mode and precursor state critically determine the phase evolution and crystallinity of sodium titanate synthesized via a sol–gel-assisted hydrothermal method at 180 °C, followed by calcination at 800 °C. Continuous hydrothermal treatment of fresh gel produces monoclinic $Na_2Ti_6O_{13}$ with a relatively small crystallite size of 12.4 nm (FWHM = 0.669°), indicating limited crystal growth and moderate structural disorder. Interrupted hydrothermal treatment also yields $Na_2Ti_6O_{13}$, but with a larger crystallite size (15.5 nm, FWHM = 0.535°), suggesting partial structural reorganization during repeated heating cycles. Pre-drying the sol–gel precursor prior to continuous hydrothermal treatment (dried gel sample) significantly enhances crystallographic ordering, yielding well-defined $Na_2Ti_6O_{13}$ with a larger crystallite size of 27.6 nm (FWHM = 0.301°). In contrast, hydrothermal treatment of the unstabilized precursor fresh gel sample) redirects phase formation toward monoclinic Na_2TiO_3 despite exhibiting a comparable crystallite size of 27.6 nm. These results confirm that crystallite size alone does not dictate phase identity; rather, phase selectivity is governed by precursor homogeneity, sodium activity, and hydrothermal kinetics. Overall, hydrothermal continuity primarily governs crystallite growth, while precursor conditioning determines phase selectivity. Controlled precursor drying combined with continuous hydrothermal processing is, therefore, essential for selectively obtaining highly crystalline $Na_2Ti_6O_{13}$ with improved structural ordering.

Acknowledgments

This research was financially supported by the Ministry of Education, Culture, Research, and Technology of the Republic of Indonesia (Kemdiktisaintek RI) through the Penelitian Dasar scheme under Contract Number 112/C3/DT.05.00/PL/2025 and Decree Number 0419/C3/DT.05.00/2025. The authors also acknowledge

Universitas Sumatera Utara and the supporting laboratories for providing facilities and technical assistance during the synthesis and characterization process.

References

[1] Ibrahim, H. A., Ayomoh, M. K., Bansal, R. C., Gitau, M. N., Yadavalli, V. S. S., & Naidoo, R. (2023). Sustainability of power generation for developing economies: A systematic review of power sources mix. In *Energy Strategy Reviews* (Vol. 47). Elsevier Ltd. https://doi.org/10.1016/j.esr.2023.101085

[2] Osman, A. I., Chen, L., Yang, M., Msigwa, G., Farghali, M., Fawzy, S., Rooney, D. W., & Yap, P. S. (2023). Cost, environmental impact, and resilience of renewable energy under a changing climate: a review. *Environmental Chemistry Letters, 21*(2), 741–764. https://doi.org/10.1007/s10311-022-01532-8

[3] Raihan, A., & Mainul Bari, A. B. M. (2024). Energy-economy-environment nexus in China: The role of renewable energies toward carbon neutrality. Innovation and Green Development, 3(3). https://doi.org/10.1016/j.igd.2024.100139

[4] Marouani, I., Guesmi, T., Alshammari, B. M., Alqunun, K., Alzamil, A., Alturki, M., & Hadj Abdallah, H. (2023). Integration of Renewable-Energy-Based Green Hydrogen into the Energy Future. Processes, 11(9). https://doi.org/10.3390/pr11092685

[5] Abo-Khalil, A. G., & Alobaid, M. (2023). A Guide to the Integration and Utilization of Energy Storage Systems with a Focus on Demand Resource Management and Power Quality Enhancement. In Sustainability (Switzerland) (Vol. 15, Issue 20). Multidisciplinary Digital Publishing Institute (MDPI). https://doi.org/10.3390/su152014680

[6] Mohd Razif, A. S., Ab Aziz, N. F., Ab Kadir, M. Z. A., & Kamil, K. (2024). Accelerating energy transition through battery energy storage systems deployment: A review on current status, potential and challenges in Malaysia. In Energy Strategy Reviews (Vol. 52). Elsevier Ltd. https://doi.org/10.1016/j.esr.2024.101346

[7] Amir, M., Deshmukh, R. G., Khalid, H. M., Said, Z., Raza, A., Muyeen, S. M., Nizami, A. S., Elavarasan, R. M., Saidur, R., & Sopian, K. (2023). Energy storage technologies: An integrated survey of developments, global economical/environmental effects, optimal scheduling model, and sustainable adaption policies. In Journal of Energy Storage (Vol. 72). Elsevier Ltd. https://doi.org/10.1016/j.est.2023.108694

[8] Abraham, K. M. (2020). How Comparable Are Sodium-Ion Batteries to Lithium-Ion Counterparts? ACS Energy Letters, 5(11), 3544–3547. https://doi.org/10.1021/acsenergylett.0c02181

[9] Hassan, Q., Algburi, S., Sameen, A. Z., Salman, H. M., & Jaszczur, M. (2023). A review of hybrid renewable energy systems: Solar and wind-powered solutions: Challenges, opportunities, and policy implications. In Results in Engineering (Vol. 20). Elsevier B.V. https://doi.org/10.1016/j.rineng.2023.101621

[10] Azizighalehsari, S., Venugopal, P., Pratap Singh, D., Batista Soeiro, T., & Rietveld, G. (2024). Empowering Electric Vehicles Batteries: A Comprehensive Look at the Application and Challenges of Second-Life Batteries. In Batteries (Vol. 10, Issue 5). Multidisciplinary Digital Publishing Institute (MDPI). https://doi.org/10.3390/batteries10050161

[11] Khan, F. M. N. U., Rasul, M. G., Sayem, A. S. M., & Mandal, N. (2023). Maximizing energy density of lithium-ion batteries for electric vehicles: A critical review. Energy Reports, 9, 11–21. https://doi.org/10.1016/j.egyr.2023.08.069

[12] Garcia, L. V., Ho, Y. C., Myo Thant, M. M., Han, D. S., & Lim, J. W. (2023). Lithium in a Sustainable Circular Economy: A Comprehensive Review. In Processes (Vol. 11, Issue 2). Multidisciplinary Digital Publishing Institute (MDPI). https://doi.org/10.3390/pr11020418

[13] Kim, H., Kim, D. Y., Zen, S., Kang, J., & Takeuchi, N. (2020). Novel Approach through the Harmonized Sulfur in Disordered Carbon Structure for High-Efficiency Sodium-Ion Exchange. ACS Applied Materials and Interfaces, 12(39), 43750–43760. https://doi.org/10.1021/acsami.0c12677

[14] Chayambuka, K., Mulder, G., Danilov, D. L., & Notten, P. H. L. (2020). From Li-Ion Batteries toward Na-Ion Chemistries: Challenges and Opportunities. Advanced Energy Materials, 10(38). https://doi.org/10.1002/aenm.202001310

[15] Lauro, S. N., Burrow, J. N., & Mullins, C. B. (2023). Restructuring the lithium-ion battery: A perspective on electrode architectures. EScience, 3(4). https://doi.org/10.1016/j.esci.2023.100152

[16] De Carolis, M., Vrankovic, D., Kiefer, S. A., Bruder, E., Dürrschnabel, M. T., Molina-Luna, L., Graczyk-Zajac, M., & Riedel, R. (2021). Towards a greener and scalable synthesis of $Na_2Ti_6O_{13}$

nanorods and their application as anodes in batteries for grid-level energy storage. Energy Technology, 9. https://doi.org/10.1002/ente.202000856

[17] Noer, Z., Sihombing, Y. A., Rajagukguk, J., Idamayanti, D., Rochliadi, A., Amri, F., & Agus, M. A. A. (2026). Effect of calcination temperature on sodium titanate properties as an anode for sodium-ion battery. Ceramics International. https://doi.org/10.1016/j.ceramint.2026.01.457

[18] Rambabu, A., Kishore, B., Munichandraiah, N., Krupanidhi, S. B., & Barpanda, P. (2017). $Na_2Ti_6O_{13}$ thin films as an anode for thin film sodium-ion batteries. AIP Conference Proceedings, 080059. https://doi.org/10.1063/1.4980519

[19] Wu, C., Wu, Z.-G., Zhang, X., Rajagopalan, R., Zhong, B., Xiang, W., Chen, M., Li, H., Chen, T., Wang, E., Yang, Z., & Guo, X. (2017). Insight into the origin of capacity fluctuation of $Na_2Ti_6O_{13}$ anode in sodium-ion batteries. ACS Applied Materials & Interfaces, 9, 43596–43602. https://doi.org/10.1021/acsami.7b11507

[20] Hu, Z., Chen, Z., Liu, Q., Zhao, W., Xu, Y., & Wu, H. B. (2023). Compact TiO_2@SnO_2@C heterostructured particles as anode materials for sodium-ion batteries with improved volumetric capacity. iScience, 26. https://doi.org/10.1016/j.isci.2023.106642

[21] Noer, Z., Sembiring, T., Sebayang, K., Nasruddin, M. N., Septawendar, R., & Sunendar, B. (2020). The effect of the calcination atmosphere in the formation of mineral sodium titanate. AIP Conference Proceedings. https://doi.org/10.1063/5.0003184

[22] Noer, Z., Sihombing, Y. A., Rajagukguk, J., Idamayanti, D., Taufik, D., Amri, F., & Agus, M. A. A. (2024). Exploring the influence of temperature on sodium titanate mineral formation using X-ray diffraction. Journal of Physics: Conference Series. https://doi.org/10.1088/1742-6596/2733/1/012017

[23] Lai, Q., Mu, J., Liu, Z., Zhao, L., Gao, X., Yang, D., Chen, H., & Luo, W. (2023). Tunnel-type $Na_2Ti_6O_{13}$@carbon nanowires as an anode material for low-temperature sodium-ion batteries. Batteries & Supercaps, 6. https://doi.org/10.1002/batt.202200549

[24] Wang, Z., Zhang, R., Chen, L., Cao, L., Guo, X., Wu, Z., Liang, B., & Luo, D. (2024). Design of $Na_2Ti_3O_7$/$Na_2Ti_6O_{13}$ nanorods for sodium-ion batteries from titanium oxysulfate solution. Journal of Electroanalytical Chemistry, 972, 1–10. https://doi.org/10.1016/j.jelechem.2024.118621

[25] Xia, Q., Liang, Y., Cooper, E. R., Ko, C.-L., Hu, Z., Li, W., Chou, S., & Knibbe, R. (2024). Monolayer sodium titanate nanobelts as a highly efficient anode material for sodium-ion batteries. Advanced Energy Materials, 14, 2400929. https://doi.org/10.1002/aenm.202400929

[26] Liu, Y., Wang, Z., Gao, L., Zhang, L., & Yang, X. (2021). Na2Ti3O7 nanosheet arrays as anode for high performance dual ion batteries. Materials Letters, 291. https://doi.org/10.1016/j.matlet.2021.129602

[27] Gao, L., Ma, Y., & Cao, M. (2024). Self-supported Se-doped Na2Ti3O7 arrays for high performance sodium ion batteries. International Journal of Hydrogen Energy, 49, 1–10. https://doi.org/10.1016/j.ijhydene.2023.07.306

[28] Basilio, L. A. L., Xavier, F., Sales, J. C. C., Andrade, J. C. S., Anglada- Rivera, J., Aguilera, L., Silva, R. S., Rodriguez-Hernandez, J., Pérez de la Cruz, J., & Leyet, Y. (2020). Fast synthesis of Na2Ti3O7 system synthesized by microwave-assisted hydrothermal method: Electrical properties. Ceramics International, 46(15), 23834–23839. https://doi.org/10.1016/j.ceramint.2020.06.160

[29] Cao, Y., Ye, Q., Wang, F., Fan, X., Hu, L., Wang, F., Zhai, T., & Li, H. (2020). A New Triclinic Phase Na2Ti3O7 Anode for Sodium-Ion Battery. Advanced Functional Materials, 30(39). https://doi.org/10.1002/adfm.202003733

[30] Idamayanti, D., Rochliadi, A., Iqbal, M., Noer, Z., Febrian, R., Septiani, N. L. W., Purwasasmita, B. S., Yuliarto, B., & Nuruddin, A. (2024). Free-standing hard carbon anode based on cellulose nanocrystal-reinforced chitosan substrate for eco-friendly sodium-ion batteries. Journal of Energy Storage, 89, 111491. https://doi.org/10.1016/J.EST.2024.111491

[31] Gao, R. M., Zheng, Z. J., Wang, P. F., Wang, C. Y., Ye, H., & Cao, F. F. (2020). Recent advances and prospects of layered transition metal oxide cathodes for sodium-ion batteries. Energy Storage Materials, 30, 9–26. https://doi.org/10.1016/j.ensm.2020.04.040